Damping Synthesis for a Spacecraft Using Substructure and Component Data

K.W. Lips* and F.R. Vigneron*
Department of Communications, Ottawa, Canada

A method for calculation of system damping factors based on solving the "general" eigenvalue problem for the motion equations, given component data as the base input information, is demonstrated. The method exhibits no computational difficulties and is confirmed by comparison to approximate results based on the Method of Averaging. The method is applied to the Hermes spacecraft, a configuration that consists of a central rigid body, two flexible solar array substructures, a momentum wheel, and a liquid-mercury damping device. The synthesized modal damping values for the structural modes vary relative to those measured in orbit by factors ranging from 0 to 5.

Nomenclature

d_1, d_2	= offset of damper from system center of mass, Fig. 1c
$\{F\}$	= forcing function applied to roll/yaw state vector, Eq. (6b)
$\underline{h}_0$	= momentum wheel bias vector
I_{ij}	= system mass moment of inertia about xyz axes
IP, OOP	= in-plane and out-of-plane, respectively
$M_\epsilon, K_\epsilon, C_\epsilon$	= substructure mass, stiffness, and damping
$J_{\bar{\alpha}}, G_{\bar{\alpha}}, C_{\bar{\alpha}}$	= matrices, respectively, associated with coordinates $\epsilon = U$, W, and $\bar{\alpha}$; Eqs. (7)
O_i	= base of array and origin of local array reference frame, Fig. 1b
Q_k	= mode shape for kth "constrained" mode
R_2, R_3	= offset of O_i relative to undeformed spacecraft center of mass, Fig. 1a
$\{S_1\}, \{S_3\}$	= integrals of assumed mode shape functions, combined as in Eqs. (7d-f)
u_i, w_i, α_i	= in-plane (x_i), out-of-plane (z_i), and twist displacement respectively
$U_i, W_i, \bar{\alpha}_i$	= time-dependent deformation coordinates for ith array, Fig. 1b
x_i, y_i, z_i	local appendage coordinates with origin at O_i, Fig. 1b
ζ_k, ω_k	= equivalent linear viscous damping ratio and frequency of kth "unconstrained" mode
λ_k	= kth eigenvalue, Eq. (8)
σ_k, Ω_k	= equivalent linear viscous damping ratio and frequency of kth "constrained" mode
$\{\Psi\}, \{\Phi\}, \{\Lambda\}$	= set of shape functions assumed for in-plane, out-of-plane, and twist deformations, respectively
ω_0	= nominal orbital angular velocity of spacecraft center of mass
$\{\ \}, [\ ]$	= column matrix, square matrix

NOTE: All damping factors are negative, but only magnitudes are presented. It is common to refer to matrix quantities without an identifying bracket.

Presented as Paper 84-1053 at the AIAA Dynamics Specialists Conference, Palm Springs, CA, May 17-18, 1984; submitted July 3, 1984; revision received March 15, 1985.

*Research Scientist. Member AIAA.

Introduction

IT is generally recognized that improvement is needed in methods for forecasting the damping characteristics of spacecraft structures in orbit. The need for improvement stems from the current trends toward spacecraft that are so large and flexible that conventional laboratory measurement of structural properties of the completely assembled spacecraft is not possible.

A method of synthesizing damping that is straightforward in principle is: 1) establish a mathematical model that includes damping for each substructure and main component, by ground test and/or analysis; 2) mathematically assemble the submodels into an overall structural model of the spacecraft; and 3) derive modal damping factors, modal frequencies, and mode shapes from the overall model by eigenproblem analysis. The method is, of course, an extension of standard practice for calculating modal frequencies and mode shapes for situations where damping can be ignored. With damping included in the procedure, a number of practical difficulties are encountered. Tractable models of damping of the subparts are difficult to establish and often are unreliable. This is particularly true for material damping in members, for components with unrestrained fluids, and for connections between structures. Differences between gravitational, thermal, and vacuum conditions in orbit and on the ground add complication and uncertainty to the process. Inadvertent omission of damping sources is a potential problem as well. Truncation of modes and off-diagonal damping matrix terms can also contribute errors. There are few documented case studies where damping factors synthesized by this type of method are compared to measured results and, hence, the degree to which this type of method is successful, and the limitations, are not yet very well established. References 1-4 and associated cited works are among the recent contributions to damping synthesis.

In Ref. 3, a method of the above-described type is applied using ground test data and compared with some of the flight results from the Hermes satellite [also known as the Communications Technology Satellite (CTS)]. In many cases, the in-orbit measured values are higher than the calculated ones by a factor of 2 or 3. Between 1976 and the end of the mission in 1980, a great deal more flight data were acquired from Hermes. These data confirm the original measurements reported in Ref. 3 and establish that the damping values are essentially constant with time. In addition, measurements for several more flexible modes are made.[5-7] Damping information on the nutational mode, with momentum wheel spinning[8] and despun,[9] is obtained as well.

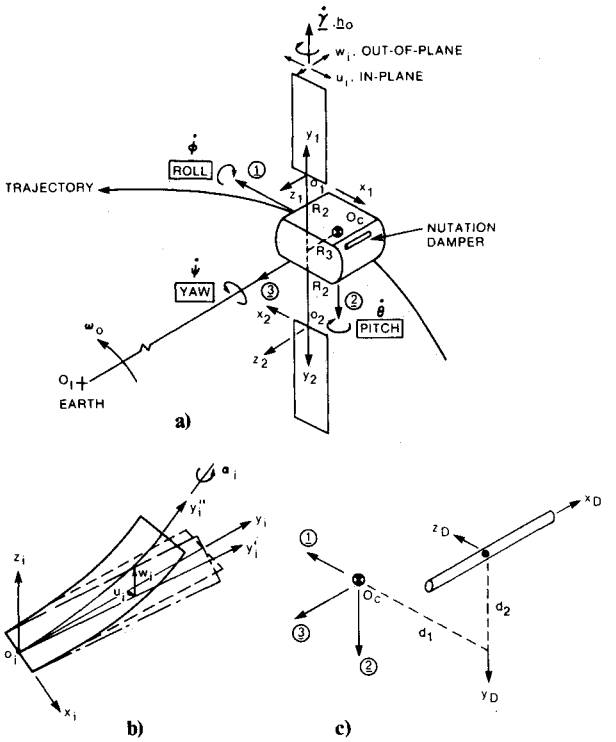

Fig. 1 Schematic for Hermes class of spacecraft: a) overall configuration, b) array coordinates, c) offset and coordinates of liquid-mercury damper.

In this paper, the synthesis method outlined above is applied to a case study of in-orbit damping characteristics of the Hermes spacecraft in the three-axis stabilized state. As well as damping, the system possesses gyroscopic stiffness. The extent to which damping in the solar array substructure and the liquid-mercury damper can be related to damping in the overall spacecraft is investigated. Of particular interest is the damping source for the nutational mode. Approximate functional relationships between component damping factors and damping of the nutational mode, based on the Method of Averaging, are used to validate the calculations associated with the eigenvalue analysis. Flight-derived modal data for Hermes are updated, summarized, and then compared with the synthesized results.

System Model

Configuration

The spacecraft consists of a central rigid body, two flexible solar arrays, a liquid-mercury damper, and a momentum wheel, configured as shown in Fig. 1. The reference frame $(Oxyz)$ is attached to the central rigid body, with O at the nominal system mass center (without deformation) of the total configuration. The arrays rotate about the Oy axis together and nominally track the sun. The central body nominally tracks the Earth. The angle between the arrays and the central body is denoted by γ, and its rate is maintained constant at 1 rev/day by a drive and track mechanism. $(O_c, \underline{1}, \underline{2}, \underline{3})$ is an orthogonal orbiting reference frame with origin fixed at the instantaneous mass center O_c, $\underline{1}$ aligned along the tangent to the trajectory in the direction of motion, $\underline{2}$ parallel to the orbit normal, and $\underline{3}$ pointing inward along the local vertical toward the center of the Earth. Thus, the frame is rotating about the Oz axis at the negative of the orbit rate $(-\omega_0)$.

Satellite attitude motion is defined by Eulerian rotations ϕ (roll), θ (pitch), ψ(yaw) of body-fixed frame (O,x,y,z) with respect to the orbit frame $(O_c,\underline{1},\underline{2},\underline{3})$. The central body rotates relative to inertial space with rates $(\omega_1,\omega_2,\omega_3)$, which in turn are related to pitch, roll, and yaw rates, to linear order, by

$$\omega_1 = \dot{\phi} - \omega_0\psi, \quad \omega_2 = \dot{\theta} - \omega_0, \quad \omega_3 = \dot{\psi} + \omega_0\phi \tag{1}$$

Component Models

Momentum Wheel

The momentum wheel is assumed to spin at constant speed, relative to the central body, and to be aligned so that its angular momentum vector $\underline{h}_0$ points in the negative Oy direction.

Liquid-Mercury Damper

The damper is a cylindrically shaped tube partially filled with mercury and aligned parallel to the predeployment spin axis, depicted schematically in Fig. 1. Detailed modeling of in-orbit performance is not straightforward and, further, is difficult to verify by ground test because of Earth gravity effects. Both geometric (size, orientation, and offset with respect to center of mass) and dynamic (mass, natural frequency, energy dissipation rate, spin rate, and gravitational field) parameters play a role in determining the damper's performance.

Originally, the Hermes damper was designed for the specific purpose of damping out the nutation associated with the spin-stabilized phase (before deployment of the arrays and start up of the momentum wheel). It was tuned to provide a maximum damping effect at about a 0.40-Hz nutation. Flight data available for this phase indicate that the nutational mode had damping ratios ranging from 0.001 to 0.007.[8]

For the spacecraft in the three-axis-stabilized phase with arrays fully deployed, the damper is excited by roll/yaw nutation, pitch axis librations, and symmetric and antisymmetric array vibrations. Specifically, the spacecraft motion consists of a combination of a slow rotation about pitch (once in 24 h), a small low-frequency nutation (0.2 deg at 2.77×10^{-3} Hz), and flexing of the various structural modes (at 0.15 Hz and higher). Relation of the damper's operation in this dynamic environment to Earth-based test or spin-phase operation is not entirely clear. In orbit, centrifugal and gravitational forces acting on the mercury are in equilibrium; hence, surface tension effects can be expected to cause the mercury to form a single slug. It is possible, for example, that the liquid-mercury damper will function as a ball-in-tube-type damper, resonant at all times with the rate of nutation. Due to the uncertainties and complexities associated with the fluid behavior, the approach adopted herein is to model the damper as a single-degree-of-freedom translational mass-spring-dashpot device (see Fig. 1). The mass (m_D) is the actual mass of the mercury and is assumed to be a slug in equilibrium at $(-d_1,-d_2)$ in $(Oxyz)$, and the dashpot and spring parameters (c_D and k_D) are selectable to match desired damper energy dissipation and resonance characteristics. Although c_D and k_D cannot be obtained with certainty for Hermes, the range of possible influence of the damper on the spacecraft can be established by varying these parameters. Such a representation is common in the literature.[10] With the nutation damper fixed in space, the kinetic, potential, and dissipation functions are, respectively,

$$\tfrac{1}{2}m_D\dot{x}_D^2; \quad \tfrac{1}{2}k_Dx_D^2; \quad \tfrac{1}{2}c_D\dot{x}_D^2 \tag{2}$$

Solar Array Substructures

Each solar array substructure is described in the overall system model by specifying its fixed-base (constrained) modal data; namely, modal frequencies (Ω), shapes (Q), and damping factors (σ). The analytic structural model for determining modal frequency and mode shape assumes that deformations are discretized in the spirit of the Rayleigh-Ritz method and is described in detail in Ref. 11. The related computer software has been extended to calculate the modal integral coefficients required in the system dynamics. A comparison of these coefficients (Table 3 of Ref. 8) and the generalized mass data indicates that the fundamental mode is dominant, thus ensuring that truncation to the first few modes will be valid.

Unlike modal frequencies and shapes, damping factors cannot be obtained using analysis only. Neither can they be measured directly in ground test, due to the difference between gravitational effects on the ground and in orbit. Consequently, a combination of 1-g test data and 1- to 0-g conver-

Table 1 Modal frequency and damping factors for the fixed-based (constrained) Hermes array as determined using ground test and adjusted by analysis to $g=0$ (Ref. 3)

Mode	Frequency	Damping ratio
Out-of-plane		
1	0.16	0.003[a]-0.006[b]
2	0.51	0.008-0.012[c]
In-plane		
1	0.32	0.014-0.020
Twist		
1	0.15	0.090-0.160
2	0.50	0.013-0.022

[a]Based on hysteretic damping law. [b]Based on viscous damping law. [c]Constructed using Table 1 of Ref. 3.

Table 2 Unconstrained modal frequency and damping ratio computed for spacecraft Hermes using damped Natural Modes Theory

Mode description	Mode No., k	Frequency ω_k, Hz	Damping ratio, ζ_k[b]
Pitch dynamics:			
Out-of-plane, symmetric	1	0.149	0.0061
Out-of-plane, symmetric	2	0.506	0.0060
Out-of-plane, symmetric	3	0.957	0.0060
Out-of-plane, symmetric	4	2.489	0.0060
Out-of-plane, symmetric	5[a]	11.600	0.0060
In-plane, symmetric	1	0.324	0.0153
In-plane, symmetric	2	3.268	0.0150
In-plane, symmetric	3[a]	19.270	0.0150
Twist, symmetric	1	0.144	0.0909
Twist, symmetric	2	0.493	0.0909
Twist, symmetric	3[a]	0.925	0.0909
Damper	–	0.400	0.0040
Roll/yaw dynamics:			
Nutation	–	0.00277	4×10^{-8}
Damper	–	0.400	0.0043
Out-of-plane, antisymmetric	1	0.444	0.0173
Out-of-plane, antisymmetric	2	0.509	0.0066
Out-of-plane, antisymmetric	3	0.970	0.0063
Out-of-plane, antisymmetric	4	2.542	0.0060
Out-of-plane, antisymmetric	5[a]	12.165	0.0060
In-plane, antisymmetric	1	0.851	0.0393
In-plane, antisymmetric	2	3.319	0.0155
In-plane, antisymmetric	3	19.300	0.0150

[a]Modes are not exact due to limitations of the Rayleigh-Ritz method used. [b]Based on input damping ratios of 0.006 out-of-plane, 0.015 in-plane, and 0.090 in twist for the constrained array substructure (Table 1) and a nominal value of 0.004 for the damper.

Table 3 Modal frequency and damping ratio as measured in-orbit on Hermes[7]

Mode No.	γ, rad	Description of mode	ω_k, Hz	ζ_k
Nutation		Roll/yaw	0.00293	0.00015
1	0	Out-of-plane, symmetric	0.150	0.030-0.038
1	0	Out-of-plane, antisymmetric	0.440	0.015-0.022
2	0	Out-of-plane, antisymmetric	0.500	0.007-0.008
1	0	In-plane, symmetric	0.300	0.030-0.039
1	0	In-plane, antisymmetric	0.820	0.012-0.016
1	$\pi/2$	In-plane, antisymmetric	0.980	
2	0	In-plane, antisymmetric	0.890	
1	0	Twist, symmetric	0.130	0.080-0.090
2	0	Twist, symmetric	0.460	

sion analysis can be tried, such as that done prior to the launch of Hermes (Table 1).

Using the model of Ref. 1, mode shapes and modal frequencies for 1-g state are obtained by solving the undamped eigenvalue problem. Experimentally measured modal frequencies and modal damping factors are also determined in ground tests. Then the analytical model and ground-test results are brought into agreement by appropriate adjustments to the analytical model.[6] In turn, this model is then used to calculate in-orbit modal frequencies and shapes by setting g equal to zero.[3,6]

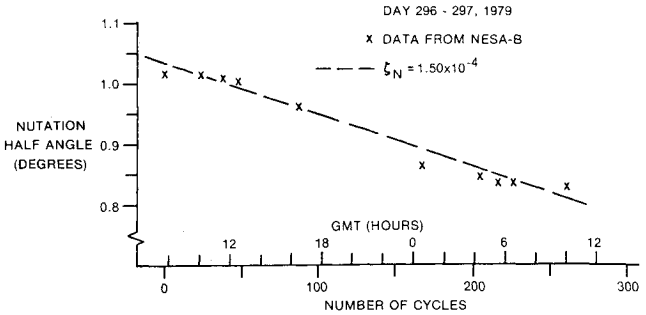

Fig. 2 Orbital data reflecting nutational decay of Hermes with arrays fully deployed.

Based on the above formulation, the kinetic, potential, and linear viscous dissipation functions are, respectively, for the north Eq. (1) array:

$$\tfrac{1}{2}\dot{U}_1^T M_U \dot{U}_1 + \tfrac{1}{2}\dot{W}_1^T M_W \dot{W}_1 + \tfrac{1}{2}\dot{\bar{\alpha}}_1^T J_{\bar{\alpha}} \dot{\bar{\alpha}}_1 \tag{3a}$$

$$\tfrac{1}{2}U_1^T K_U U_1 + \tfrac{1}{2}W_1^T K_W W_1 + \tfrac{1}{2}\bar{\alpha}_1^T G_{\bar{\alpha}} \bar{\alpha}_1 \tag{3b}$$

$$\tfrac{1}{2}\dot{U}_1^T C_U \dot{U}_1 + \tfrac{1}{2}\dot{W}_1^T C_W \dot{W}_1 + \tfrac{1}{2}\dot{\bar{\alpha}}_1^T C_{\bar{\alpha}} \dot{\bar{\alpha}}_1 \tag{3c}$$

It is convenient to transform to "symmetric" and "antisymmetric" coordinates. For example, for the in-plane degrees of freedom,

$$U_s = \tfrac{1}{2}(U_1 - U_2); \quad U_a = \tfrac{1}{2}(U_1 + U_2) \tag{4}$$

Equations of Motion

Second-order equations governing the attitude motion (pitch, roll, and yaw) and array vibrations for the Hermes-type configuration of Fig. 1a, just described, are well documented.[12,13] In the absence of a damper, symmetries inherent in the configuration serve to uncouple dynamics of pitch from roll and yaw. In addition, symmetric array oscillations interact with pitch only and vice versa. Similarly, roll/yaw degrees of freedom interact only with antisymmetric bending vibrations and vice versa. This paper extends the above representation to account for the liquid-mercury damper. With the damper included, roll/yaw and pitch are, in general, coupled. If offset d_1 is nonzero and offset d_2 is zero, the damper couples to pitch but not roll/yaw; if d_1 is zero and d_2 is nonzero the damper couples to roll/yaw, but not to pitch. To aid in isolating the effect of the damper, this study is confined to these bounding cases. The complete second-order system of equations for this case is contained in Ref. 8.

Following the approach outlined in Ref. 14, which is similar to that of Ref. 15, the equations are transformed to a first-order set through introduction of a state vector made up of generalized displacement and generalized velocity. By choosing a suitable constraint between generalized velocity and displacement, system matrices are rendered symmetric, or skew symmetric. Algebraic manipulation is used to avoid use of complex numbers when generating a response from the resulting eigenvalue problem and its adjoint. Once system eigenvalues and eigenvectors are known, response depends on the solution of coupled, real-valued, scalar, first-order equations. For the roll/yaw dynamics, the state vector chosen is

$$\{z\} = \{\omega_1 \;\; \omega_3 \;\; \dot{U}_a^T \dot{W}_a^T \dot{x}_D U_a^T W_a^T x_D\}^T \tag{5}$$

The transformed equations then take the form

$$[A]\{\dot{z}\} + [B]\{z\} = \{F\} \tag{6a}$$

where

$$\{F\} = \{L_1 L_3 0\;0\;0\;0\;0\;0\}^T \tag{6b}$$

$$[A]=\begin{bmatrix} I_{11} & I_{13} & -2\sin\gamma S_1^T & -2\cos\gamma S_3^T & -m_D d_2 & 0 & 0 & 0 \\ I_{13} & I_{33} & -2\cos\gamma S_1^T & 2\sin\gamma S_3^T & 0 & 0 & 0 & 0 \\ -2\sin\gamma S_1 & -2\cos\gamma S_1 & 2M_U & 0 & 0 & 0 & 0 & 0 \\ -2\cos\gamma S_3 & 2\sin\gamma S_3 & 0 & 2M_W & 0 & 0 & 0 & 0 \\ -m_D d_2 & 0 & 0 & 0 & m_D & 0 & 0 & 0 \\ 0 & 0 & 0 & 0 & 0 & 2K_U & 0 & 0 \\ 0 & 0 & 0 & 0 & 0 & 0 & 2K_W & 0 \\ 0 & 0 & 0 & 0 & 0 & 0 & 0 & k_D \end{bmatrix} \quad (6c)$$

$$[B]=\begin{bmatrix} 0 & h_0 & 0 & 0 & 0 & 0 & 0 & 0 \\ -h_0 & 0 & 0 & 0 & 0 & 0 & 0 & 0 \\ 0 & 0 & 2C_U & 0 & 0 & 2K_U & 0 & 0 \\ 0 & 0 & 0 & 2C_W & 0 & 0 & 2K_W & 0 \\ 0 & 0 & 0 & 0 & c_D & 0 & 0 & k_D \\ 0 & 0 & -2K_U & 0 & 0 & 0 & 0 & 0 \\ 0 & 0 & 0 & -2K_W & 0 & 0 & 0 & 0 \\ 0 & 0 & 0 & 0 & -k_D & 0 & 0 & 0 \end{bmatrix} \quad (6d)$$

Also, assuming shape functions $\{\Psi\}$ and $\{\Phi\}$ for in-plane and out-of-plane deformations,

$$M_U=\int\Psi\Psi^T dm; \qquad M_W=\int\Phi\Phi^T dm \quad (7a)$$

$$K_U=\Omega_U^2 M_U; \qquad K_W=\Omega_W^2 M_W \quad (7b)$$

$$C_U=2M_U\Omega_U\sigma_U; \qquad C_W=2M_W\Omega_W\sigma_W \quad (7c)$$

$$B_1=\int y\Psi dm; \qquad B_3=\int y\Phi dm \quad (7d)$$

$$D_1=\int\Psi dm; \qquad D_3=\int\Phi dm \quad (7e)$$

$$S_1=B_1+R_2D_1; \qquad S_3=B_3+R_2D_3 \quad (7f)$$

The associated eigenvalue problem for Eq. (6a) (taking $L_1=L_3=0$) is

$$(\lambda_k[A]+[B])\{X_k\}=\{0\} \quad (8)$$

The development for the symmetric pitch dynamics is analogous and the relevant equations are available in Ref. 8.

Based on this formulation, computer software is developed to solve for system natural modes, frequencies, and damping factors for both the roll/yaw and pitch dynamics. Results computed using the roll/yaw software are demonstrated for the Hermes satellite configuration of Fig. 1, in Table 2. A set of nominal input parameters is assigned, which includes the measured/computed modal characteristics for the constrained array, together with the spin-phase damper design characteristics ($m_D=0.1145$ kg, $\Omega_D=0.40$ Hz, $\sigma_D\simeq 0.004$).[8] The frequencies calculated agree quite well with those published in Refs. 5 and 7, and other works, thus validating the software. No numerical or computational problems are experienced with the method.

Update of Measured Hermes Data

Measurements of natural frequency and damping factor for the vibrational modes of the Hermes satellite are reported in Refs. 3, 5, and 7, and other unpublished internal reports. The in-orbit data are derived from residual oscillations associated with array deployment and slewing, and from specially implemented excitation (SPEX) by the thrusters. Damping factors are deduced from the decay envelope of free vibration (log decrement method) and from the sharpness given by the Fourier transform of the vibrational data.

To obtain a single and updated consistent set of in-orbit values, both published and unpublished data were reviewed. Table 3 summarizes the results. For most modes reported, the accelerometer data from which the results are deduced is of excellent quality, and the confidence level in the measurements is rated high. For the second out-of-plane antisymmetric mode, the accelerometer data are of lower quality and the confidence level is rated medium.

Late in the mission, an in-orbit dynamics test was carried out to establish the characteristics of nutation in the three-axis-stabilized mode. A nutation cone of 1 deg was initiated, the thrusters were inhibited, and the satellite was allowed to nutate without disturbance for 12 h. Data from the tests are reproduced in Fig. 2. The nutation period and damping ratio are measured to be 341 s and 1.5×10^{-4}, respectively (see Table 3). Good agreement exists between the measured and calculated nutation frequencies.

Parametric Assessment of Component Damping Effect

Once in orbit, there exists a degree of uncertainty as to what level of damping to use for the components. Whereas damper mass and offsets are well known, σ_D and Ω_D are not. Similarly, in the modal representation for the array, the exact level of damping associated with each mode and the effect of mode truncation are not known with confidence. By first isolating and then varying these parameters, their range of possible influence on the spacecraft can be determined. For the case of the damper this includes varying frequency, in addition to damping, in order to simulate resonance with either the array vibration or nutation. A special case for the arrays involves determining the effect of critical damping in the constrained mode input. This knowledge of system sensitivity to inputs at the component level is helpful in understanding the flight-derived data.

Role of the Array Substructure

To establish the degree to which damping factors measured in orbit can be attributed to damping sources in the arrays, σ_D is set equal to zero and computer runs are made using, for damping input, those values as determined from the ground-based substructure test results of Table 1, along with variations as adopted in Table 4.

It is seen, from Table 4, that the inherent damping of the arrays has little influence on damping of the system nutation. Input modal damping parameters σ_k associated with the substructure are varied between 0.001 and 0.100. Over this range, when there is in-plane damping only, a nutation damping of $\zeta_N=5\times10^{-10}$ and 10^{-8}, respectively, results (i.e., ζ_N is proportional to $\sigma_{k,\mathrm{IP}}$). On the other hand, input damping associated with array out-of-plane motions only is seen to

Table 4 Contribution of array substructure to damping of system roll/yaw modes

Array substructure input damping						Output modal damping							
In-plane			Out-of-plane			Nutation	In-plane			Out-of-plane			Damper
σ_1	σ_2	σ_3	σ_1	σ_2	σ_3	ζ_N	ζ_1	ζ_2	ζ_3	ζ_1	ζ_2	ζ_3	ζ_D
0.001	0.001	0.001				5×10^{-10}	2.6×10^{-3}	1×10^{-3}	1×10^{-3}	1×10^{-6}	1×10^{-7}	6×10^{-7}	1×10^{-9}
0.100	0.100	0.100				5×10^{-8}	2.7×10^{-1}	1.04×10^{-1}	1.01×10^{-1}	1×10^{-4}	9×10^{-6}	1×10^{-5}	1×10^{-7}
			0.001	0.001	0.001	6×10^{-9}	2×10^{-6}	7×10^{-10}	4×10^{-13}	2.9×10^{-3}	1.1×10^{-3}	1.1×10^{-3}	4×10^{-6}
			0.100	0.100	0.100	6×10^{-7}	1×10^{-4}	7×10^{-8}	4×10^{-11}	3.1×10^{-1}	1.04×10^{-1}	1.05×10^{-1}	4×10^{-5}
0.100	0.100	0.100	0.100	0.100	0.100	6×10^{-7}	2.7×10^{-1}	1.04×10^{-1}	3.0×10^{-1}	1.1×10^{-1}	1.04×10^{-1}	1.06×10^{-1}	4×10^{-5}
0.020	0.020	0.020				1×10^{-8}	5.2×10^{-2}	2.1×10^{-2}	2×10^{-2}	2×10^{-5}	2×10^{-6}	1×10^{-5}	2×10^{-8}
0.020	0.020	0.020	0.006	0.006	0.006	5×10^{-8}	5.2×10^{-2}	2.1×10^{-2}	2×10^{-2}	1.7×10^{-2}	6.6×10^{-3}	6.6×10^{-3}	2×10^{-5}
0.020			0.006	0.010		5×10^{-8}	5.2×10^{-2}	4×10^{-4}	6×10^{-6}	1.7×10^{-2}	1×10^{-2}	3×10^{-4}	2×10^{-4}
0.020	1.0	1.0	0.006	0.010	1.0	5×10^{-8}	5.3×10^{-2}	1	1	1.9×10^{-2}	1×10^{-2}	1	2×10^{-5}
0.020	0.020	0.020				6×10^{-9}	5.2×10^{-2}	2.1×10^{-2}	2×10^{-2}	2×10^{-5}	2×10^{-6}	1×10^{-5}	5×10^{-9}
1.0						3×10^{-7}	1	6×10^{-3}	3×10^{-4}	8×10^{-5}	4×10^{-6}	2×10^{-6}	2×10^{-7}
	1.0					1×10^{-12}	4×10^{-4}	1	1×10^{-5}	4×10^{-9}	1×10^{-9}	2×10^{-7}	1×10^{-12}
1.0	1.0	1.0				3×10^{-7}	1	0.98[a]	1	8×10^{-5}	4×10^{-6}	2×10^{-6}	2×10^{-7}

[a] $(\omega_2)_{IP} = 0.58$ Hz for this case.
Note: $m_D = 0.1145$ kg; $\sigma_D = 0$; $d_1 = 0$; $d_2 = -0.29$ m. Blank entires are zero.

have an effect an order of magnitude greater which, however, is still not significant when compared with the measured level of $\zeta_N = 1.5\times10^{-4}$. The overall effect on ζ_N is no greater when in-plane and out-of-plane damping inputs are combined. Also, using input damping ratios consistent with typical ground-based array measurements still results in an insignificant effect on the nutation, i.e., $\zeta_N \simeq 5\times10^{-8}$, in this case.

Table 4 also provides information about the relationship between damping ratio for unconstrained antisymmetric modes (ζ_k) and the input damping associated with the constrained arrays (σ_k). It is seen that, when the substructure is damped in-plane only, the system damping is greatest in-plane as well. The same holds true for the out-of-plane degrees of freedom. Specifically, the magnitudes of damping calculated for these modes, referred to as the second and third system modes in-plane or out-of-plane, are very close to the levels of damping input for the second and third substructure modes. However, damping computed for the first modes, in each category of motion, is significantly larger than the damping input for the fundamental mode of the array alone. This is consistent with the nature of the dynamic interactions occurring for this class of spacecraft and is analogous to the differences in frequencies recorded between the system and subsystem data.[8] In addition, note that the presence of a nonzero out-of-plane damping input gives rise to nonzero damping ratios for unconstrained in-plane modes and vice versa (i.e., if $\sigma_{k,IP} = 0.10$ or $\sigma_{k,OOP} = 0.10$, then $\zeta_{1,OOP} = 1\times10^{-4}$ or $\zeta_{1,IP} = 1\times10^{-4}$). In a similar parametric study carried out using software developed for the pitch dynamics, it was found that modal damping of the symmetric spacecraft modes remains very close to that input for a single constrained array (within 2%).

The techniques used for measuring damping, as explained earlier, depend on having an oscillatory response. It is possible that a critically damped or overdamped substructure mode could be missed in the test results or truncated. This issue is addressed for the roll/yaw dynamics in Table 4. For example, $\sigma_k = 1.0$ for the fundamental constrained in-plane mode yields unconstrained damping ratios for the first, second, and third in-plane modes which are critical, 0.006, and 0.0003, respectively. That is, the degree of intermodal coupling in damping is slight. This is found to be the case also if the higher modes are input with critical damping. A similar situation exists for the pitch dynamics. It is implied by such behavior that the ζ's of spacecraft modes measured in orbit are not sensitive to the input σ's of those higher-order, and, in most instances, unmeasured, modes.

Role of the Liquid-Mercury Damper

To isolate the effect of the damper, input damping associated with the array substructures is set equal to zero.

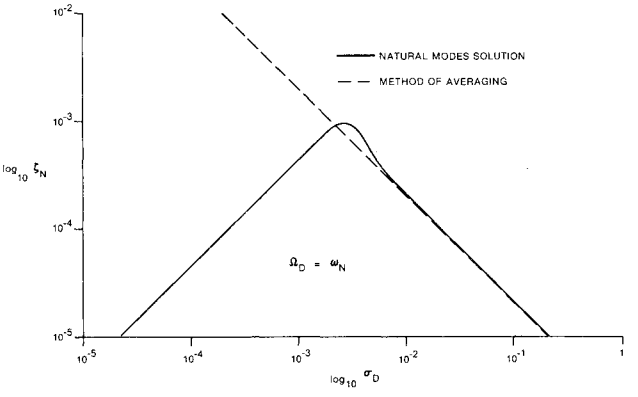

Fig. 3 Calculated nutation damping of Hermes for the case of a resonant damper.

The approach then is to vary Ω_D and σ_D over a wide range in order to ascertain the theoretical limits for the damper's effect on spacecraft damping in orbit.

A parametric study using the roll/yaw software yields the following results. When damper input frequency (Ω_D) is away from the nutation frequency ($\omega_N = 0.00277$ Hz), the damping factor of the system nutation remains extremely small (10^{-12}), even if damping input associated with the damper itself becomes large (e.g., $\sigma_D = 0.5$). As Ω_D approaches ω_N, the influence of the damper, although still small, nevertheless increases noticeably (i.e., for $\Omega_D = 0.0015$ Hz and $\sigma_D = 0.006$, $\zeta_N = 5\times10^{-8}$). If the damper component frequency is set equal to the nutation rate, a resonant condition exists and the effect on level of nutation damping is dramatic, as shown in Fig. 3 where $\Omega_D = \omega_N$ and $10^{-5} < \sigma_D < 1$. Over this range of input ζ_N achieves a maximum value of 9×10^{-4}, which is comparable to the flight-determined level of 1.5×10^{-4}.

The calculated nutation damping factors extend over at least eight orders of magnitude, thus raising concern about whether or not the software-generated data are reliable over such a wide range. For this reason, the following approximate formulas are derived by the Method of Averaging,[8] and applied to check the software:

$$\zeta_N \simeq \frac{1}{4}\left(\frac{m_D d_2^2}{I}\right)\left(\frac{1}{\zeta_D}\right) \qquad \text{when } \omega_N = \omega_D \qquad (9a)$$

$$\zeta_N \simeq \frac{1}{4}\left(\frac{m_D d_2^2}{I}\right)\left(\frac{\omega_N}{\omega_D}\right)^3 \zeta_D \qquad \text{when } \omega_N \ll \omega_D \qquad (9b)$$

Results from the two methods are compared in Fig. 3 for the resonant case. It is seen that the Method-of-Averaging data

Table 5 Measured vs calculated damping factors

Mode description	Calculated[a] ζ_k; σ_k from ground-based data[b]		Calculated[a] ζ_k; σ_k derived from in-orbit symmetric modes[c]		Flight-measured ζ_k (Table 3)
	Viscous	Hysteretic	Viscous	Hysteretic	
Nutation	4×10^{-8}	2×10^{-6}	2×10^{-7}	1×10^{-5}	1.5×10^{-4}
1st symmetric, out-of-plane	0.0061	0.0061	0.0305	0.0305	0.030-0.038
1st symmetric, in-plane	0.0153	0.0163	0.0305	0.0325	0.030-0.039
1st symmetric, twist	0.0909	0.0977	0.0806	0.0868	0.080-0.090
1st antisymmetric, out-of-plane	0.0173	0.0059	0.0872	0.0297	0.015-0.022
2nd antisymmetric, out-of-plane	0.0066	0.0067	0.0328	0.0335	0.007-0.008
1st antisymmetric, in-plane	0.0393	0.0153	0.0788	0.0308	0.012-0.016

[a]Damping from array substructure only, $\sigma_D = 0$. [b]0.015 in-plane, 0.006 out-of-plane, and 0.090 in twist. [c]0.030 in-plane, 0.030 out-of-plane, and 0.080 in twist.

yield excellent agreement with the software calculations over the range $0.001 \le \sigma_D \le 0.100$ and, thus, confirm operation of the software. Note, however, for the Method of Averaging to work the degree of interaction must be weak. The analysis of Ref. 8 (Appendix A) shows that this is not the case at resonance when the damper is very lightly damped. In particular, from Fig. 3, it is seen that the exact formulation is required when dealing with levels of damper input smaller than 10^{-3}. Away from resonance, the methods agree reasonably well. At $\omega_D = 0.020$ Hz and $\zeta_D = 0.005$, ζ_N becomes 3×10^{-11} and 10×10^{-11} when computed by the Method of Averaging [Eq. (9b)] and the Natural Modes Theory, respectively.

The functional relationships described by Eqs. (9) show, as well, that damper effectiveness in increasing the ζ_N output is proportional to m_D and varies quadratically with the offset geometry d_2. A similar set of relations applies to the effect of substructure damping input on ζ_N.

The effect of the damper on other system modes is small. With $\sigma_D = 0.5$ and damper frequencies either near or removed from the nutation resonance condition, the output damping ratios for the antisymmetric modes remain less than 10^{-6}. The only exception occurs for $\Omega_D = \omega_{1,\text{OOP}} = 0.44$ Hz, where, if $\sigma_D = 0.1$, then $\zeta_{1,\text{OOP}} = 2\times10^{-4}$, which is still considerably less than the measured values of 0.015-0.022. For the symmetric modes the greatest damper effect occurs with the damper tuned to be near resonance with the first twist mode. In this case, a maximum damping ratio of only 10^{-5} is found for the fundamental twist mode over the input range $0.001 \le \sigma_D \le 0.100$—significantly less than the flight-measured values of 0.08-0.09.

In summary, it can be concluded that 1) the liquid-mercury damper could have contributed the damping of the nutational mode, however, to do so the fluid would have had to be excited to resonance by the nutations; and 2) the damper did not contribute significantly to the damping factors of either the symmetric or antisymmetric vibrational modes.

Correlation of Computed and Flight-Derived Modal Damping

In Table 5, damping factors measured in orbit are compared to corresponding ones synthesized from substructure component damping. The damper is not included in this comparison because its influence has already been discussed in detail in the parameter study, where it was found that it can be a significant factor only when resonant with the nutations.

For one set of calculations the input damping adopted is the nominal ground-test-derived damping of the constrained array. The substructure modeling assumes an equivalent linear viscous modal damping process. The results computed are contained in the first data column of Table 5 and originate in Table 2. When compared with the flight-measured information, it is seen that agreement is quite good for the first and second antisymmetric out-of-plane modes and for the fundamental symmetric twist modes. The nutation, the first out-of-plane symmetric, as well as first in-plane symmetric and antisymmetric modes, however, do not correlate well.

A possible reason that agreement is poor in some cases, is that the viscous model put forth for array damping is inadequate. An alternative is the hysteretic model for which the damping coefficient, rather than being a constant, varies inversely with the frequency. Calculations carried out using a hysteretic model and the nominal ground-based array damping input give the results contained in the second data column of Table 5. Although both nutational damping and the damping for the first antisymmetric in-plane mode compare more favorably with the measured result, there is no consistent improvement in correlation achieved with this approach.

Another attempt is made to improve the calculated result by revising the input damping factors. Since input-constrained modes are very similar to the flight-measured symmetric unconstrained modes (the spacecraft central body is heavy relative to the arrays and is essentially a fixed base in orbit), it is logical to try, as the input σ's, the corresponding flight-measured symmetric ζ's. The runs corresponding to this concept are listed in Table 5 as well, for both viscous and hysteretic models. As would be expected, the ζ's for the symmetric modes match the flight data well. However, the antisymmetric modal damping correlation is considerably poorer. Again the hysteretic model does not result in any consistent improvement over the viscous prediction.

Conclusions

A Natural Modes approach is used to synthesize the component and substructure damping of a spacecraft into the system-level damping factors associated with the damped gyroscopic modes. The method is seen to be systematic and to have no computational instabilities. The functional relationships between component damping factors and the damping factor for the nutational mode, as derived by the Method of Averaging, confirm the functioning of the computer software developed for the eigenvalue analysis.

The performance of the method is demonstrated by applying it to the Hermes data. All synthesized modal frequencies agree with flight data and, thus, are consistent with previously reported works based on models with no damping. Ignoring the special case for nutation, the synthesized modal damping factors are found to differ relative to those measured in orbit by factors ranging from 0 to 5. Also excluding the nutation mode, the source of damping for the system-level modes is the structural damping of the solar array. On the other hand, it is the liquid-mercury damper that likely contributed to damping of the nutational mode.

The agreement achieved between measured and synthesized damping factors is similar to that of the few earlier published works. Shortcomings in correlation could be due to inadequacies in the law chosen to model damping of the solar arrays, or possibly, to omission of a damping source (such as friction between the substructures).

References

[1]Kana, D.D. and Huzar, S., "Synthesis of Shuttle Vehicle Damping Using Substructure Test Results," *Journal of Spacecraft and Rockets,* Vol. 10, Dec. 1973, pp. 790-797.

[2]Hasselman, T.K., "Damping Synthesis for Substructure Tests," *AIAA Journal,* Vol. 13, Oct. 1976, pp. 1409-1418.

[3]Vigneron, F.R., "Ground-Test Derived and Flight Values of Damping for a Flexible Spacecraft," *Proceedings of the Symposium on Dynamics and Control of Non-Rigid Spacecraft,* Frascati, Italy, May 1977, ESA-SP-117, pp. 325-333.

[4]Santini, P., Castellani, A., and Nappi, A., "An Introduction to the Problem of Dynamic Structural Damping," AGARD Rept. 663, Jan. 1978.

[5]Vigneron, F.R., "Dynamics, Control and Structural Flexibility Results from the Hermes Mission," *Astronautics for Peace and Human Progress,* Pergamon Press, New York, 1979, pp. 397-411.

[6]Vigneron, F.R. and Hughes, P.C., "Structural Dynamics Modelling for Hermes – Modelling and Measurement," *Hermes (The Communication Technology Satellite) Its Performance and Applications, Proceedings of the Royal Society of Canda, 20th Symposium,* 1977, IBSN0-920064-12-4.

[7]Garg, S.C., Hughes, P.C., Millar, R.A., and Vigneron, F.R., "Flight Results on Structural Dynamics from Hermes," *Journal of Spacecraft and Rockets,* Vol. 16, March-April 1979, pp. 81-87.

[8]Lips, K.W. and Vigneron, F.R., "Damping Synthesis for a Spacecraft Structure Using Substructure and Component Data," Department of Communications, Ottawa, Canada, CRC Rept. 1365, Aug. 1984.

[9]Vigneron, F.R. and Krag, W.E., "Optical Measurements and Attitude Motion of Hermes After Loss of Stabilization," *Journal of Guidance, Control, and Dynamics,* Vol. 5, Sept.-Oct. 1982, pp. 539-541.

[10]Cochran, J.E. Jr. and Thompson, J.A., "Nutation Dampers vs Precession Dampers for Asymmetric Spacecraft," *Journal of Guidance and Control,* Vol. 3, Jan.-Feb. 1980, pp. 22-28.

[11]Vigneron, F.R., "A Structural Dynamics Model for Flexible Solar Arrays of the Communications Technology Satellite," Department of Communications, Ottawa, Canada, CRC Rept. 1268, April 1975.

[12]Hughes, P.C., "Flexibility Considerations for the Pitch Attitude Control of the Communications Technology Satellite," *CASI Transactions,* Vol. 5, No. 1, March 1972.

[13]Hughes, P.C., "Attitude Dynamics of a Three-Axis Stabilized Satellite with a Large Flexible Solar Array," *Journal of the Astronautical Sciences,* Vol. XX, No. 3, Nov.-Dec. 1972, pp. 166-189.

[14]Vigneron, F.R., "Natural Modes and Real Modal Variables for Flexible Spacecraft," Department of Communications, Ottawa, Canada, CRC Rept. 1348, Nov. 1981.

[15]Meirovitch, L. and Baruh, H., "Optimal Control of Damped Flexible Gyroscopic Systems," *Journal of Guidance and Control,* Vol. 4, March-April 1981, pp. 157-163.